IFP Energies nouvelles International Conference
Rencontres Scientifiques d'IFP Energies nouvelles

Deep Saline Aquifers for Geological Storage of CO_2 and Energy
Stockage géologique du CO_2 et de l'énergie en aquifères salins profonds

Sequential Model Coupling for Feasibility Studies of CO_2 Storage in Deep Saline Aquifers

M. Darcis*, H. Class, B. Flemisch and R. Helmig

Department of Hydromechanics and Modeling of Hydrosystems, Universität Stuttgart, Pfaffenwaldring 61, 70569 Stuttgart - Germany
e-mail: melanie.darcis@iws.uni-stuttgart.de - holger.class@iws.uni-stuttgart.de - bernd.flemisch@iws.uni-stuttgart.de
rainer.helmig@iws.uni-stuttgart.de

* Corresponding author

Résumé — **Couplage séquentiel des modèles numériques appliqué aux études de faisabilité du stockage de CO_2 en aquifère salin profond** — Simuler numériquement, à l'échelle du réservoir, le stockage de dioxyde de carbone (CO_2) en aquifère salin profond est très exigeant en temps calcul. Des scénarios réalistes demandent en effet que soit prise en compte, avec assez de détail, la distribution géométrique hétérogène des propriétés. En outre, les mécanismes physiques à représenter sont très complexes. Les modèles numériques doivent intégrer les processus compositionnels, multi-phases, et non isothermes, qui surviennent durant le stockage. Cependant, en général, il n'est pas indispensable de décrire la totalité des processus physiques tout au long de la période de temps à simuler. Selon l'étape du stockage, les phénomènes dominants changent. Ce comportement des systèmes réels permet d'adapter les modèles en réduisant leur complexité, tout en capturant bien, à chaque étape, les processus majeurs. On montre ici qu'en couplant des modèles de complexité réduite, on augmente l'efficacité numérique du modèle d'ensemble sans négliger les phénomènes pertinents. Ce couplage séquentiel des modèles représente un premier jalon sur la voie d'une efficacité accrue de la modélisation numérique.

Abstract — Sequential Model Coupling for Feasibility Studies of CO_2 Storage in Deep Saline Aquifers – Modelling carbon dioxide (CO_2) storage in saline aquifers on a reservoir scale is very demanding with respect to computational cost. In realistic scenarios, large heterogeneous geometries need to be described. In addition, the governing physical processes are very complex. The models need to take into account nonisothermal, multiphase, and compositional processes that occur during CO_2 storage. However, in most cases, it is not necessary to describe all the physical processes for the whole simulation time period. The processes which dominate during CO_2 storage operations vary over time. This time-dependent behaviour allows for the use of models of reduced/adapted complexity for the description of the dominant processes within a given timescale. It is shown that by coupling these models of reduced complexity, the model efficiency can be increased without neglecting the relevant phenomena. Sequential coupling of models thus represents a first step in the direction of increased model efficiency.

NOMENCLATURE

κ	Component index, either H_2O or CO_2
α	Phase index, either brine phase (w) or CO_2-rich phase (*n*)
ϕ	Porosity (-)
ρ_α	Phase density (kg/m^3)
μ_α	Phase viscosity (Pa·s)
$k_{r\alpha}$	Relative permeability of phase α (-)
λ_{pm}	Heat conductivity of the porous medium (W/(m·K))
λ_{dry}	Porous media heat conductivity for $S_w = 0$ (W/(m·K))
λ_{sat}	Porous media heat conductivity for $S_w = 1$ (W/(m·K))
λ_{BC}	Brooks-Corey parameter
S_α	Phase saturation (-)
X_α^κ	Mass fraction of the component κ in the phase α (-)
X_{eq}^κ	Mass fraction of the component κ in case of thermodynamic equilibrium (-)
K	Intrinsic permeability (m^2)
g	Gravity (m/s^2)
$\mathbf{D}_{\alpha,\mathbf{pm}}^\kappa$	Diffusion coefficient of the component κ in the phase α in the porous medium (m^2/s)
p_α	Phase pressure (Pa)
p_c	Capillary pressure (Pa)
p_d	Brooks-Corey entry pressure (Pa)
u_α	Specific internal energy of phase α (J/kg)
h_α	Specific enthalpy of phase α (J/kg)
c_s	Specific heat capacity of the rock (J/kg·K)
$q_\alpha, q_h, q_\alpha^\kappa$	Source or sink term of phase α, heat or component κ

INTRODUCTION

After more than ten years of research the CCS (Carbon Capture and Storage) technology is currently in the stage of large-scale demonstration projects. For the realisation of these projects, a responsible identification and characterisation of suitable CO_2 storage sites is crucial. In order to identify appropriate storage sites, detailed geological data is required. Apart from geological information, modelling tools are needed that are capable of describing complex hydraulic, thermal, geomechanical, and geochemical processes on a large range of spatial and temporal scales.

In recent years, different modelling tools have been developed which describe the thermal and hydraulic processes during CO_2 storage. Class *et al.* (2009) give an overview of existing simulators and discuss an intercomparison study by means of three benchmark problems related to CO_2 storage. The temporal scale of the benchmark examples was limited to a period of 50 years and the spatial scale did not exceed 10 km (*i.e.*, reservoir scale).

For investigations on pressure build-up and brine migration, reservoir extensions on scales of more than 100 km need to be modelled. Besides the computational requirements with respect to model domain size, the simulation of CO_2 storage might need to cover large timescales depending on the problem that needs to be solved. With respect to the risks of CO_2 storage and sustainability of the storage, the fate of the injected CO_2 plume needs to be modelled over very long periods (thousands of years). Such large-scale and long-term simulations were recently addressed by a follow-up benchmark study (http://org.uib.no/cipr/Workshop/2009/CO2/Benchmark.htm).

Thus, the scales required for the simulation of realistic storage scenarios are already computationally demanding, even when the model concepts are restricted to flow and transport processes of the CO_2 in the reservoirs. However, geomechanical and geochemical processes can become very relevant in certain cases with respect to risk estimation. Such additional processes increase the number of unknowns and thus the computational costs enormously.

Most of the existing simulators are not capable of describing all the potentially relevant physical and/or chemical processes. In particular, when adding geochemistry to the flow and transport model concepts, the computation times for solving large-scale systems increase dramatically. Therefore, these models are often restricted to simplified geometries or small timescales.

One possibility to overcome this problem could be the coupling of different models. Provided that it is possible to identify distinctly dominant processes in subdomains or during certain time periods, it can be a good strategy to model only these processes for the given regions or times (Darcis *et al.*, 2009).

This manuscript focuses particularly on the sequential coupling of models with the aim of efficiently simulating the short and long-term behaviour of a CO_2 plume in a storage reservoir. A detailed description of the different time periods that can be distinguished during and after the injection of CO_2 into a geologic reservoir is given in Section 1. A sequential coupling concept is presented in Section 2 and an idealised example application is described in Section 3. The results of the application example and two additional variations, taking into account the effects of heterogeneities and grid refinement, are presented and discussed in Section 4, followed by some concluding remarks and perspectives.

1 MOTIVATION FOR MODEL COUPLING

Several characteristic time periods can be distinguished during and, in particular, after the injection of CO_2 into a geologic reservoir (*see Fig. 1*). In the following, this is discussed for a hypothetical injection into a saline aquifer.
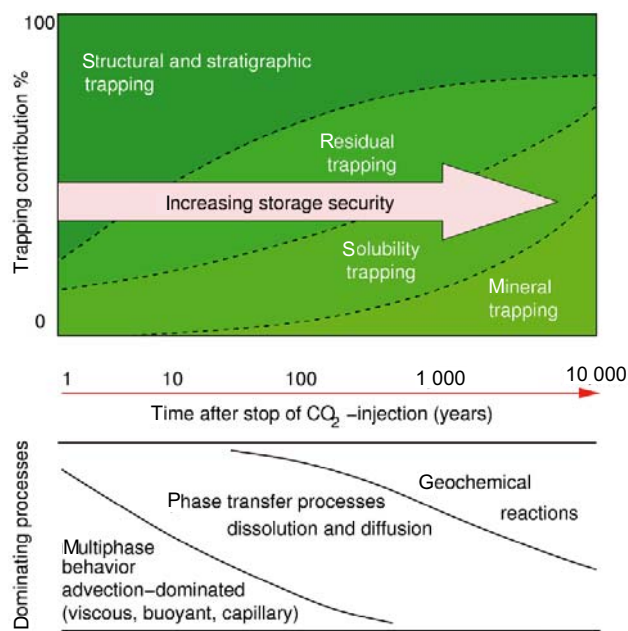
Figure 1

Trapping mechanisms and governing processes during and after the injection of CO$_2$ into saline aquifers (modified after IPCC Special Report, 2005).

In the injection stage, the low mutual solubilities of brine and CO$_2$ lead to the formation of a multiphase flow system which is driven by large pressure gradients, strong viscous and buoyant forces. Close to the injection well, large changes in pressure increase the relevance of geomechanical processes (deformation). Changes in porosity and permeability or even enlargement of faults or generation of fractures in the caprock might occur. Alterations in hydraulic parameters might also occur due to salt precipitation close to the injection well. The injected CO$_2$-rich phase is generally undersaturated with respect to water (H$_2$O) under reservoir conditions. Thus, H$_2$O evaporates from the saline brine into the CO$_2$-rich phase, the concentration of the dissolved salts in the residual brine phase increases until finally salt precipitates. Due to the evaporation of H$_2$O a single-phase CO$_2$ region evolves in the vicinity of the well.

At early times, temperature changes can affect fluid and rock properties. These temperature changes can be caused by a downhole temperature of the injected CO$_2$, which differs from the reservoir temperature. Moreover, the Joule-Thompson effect leads to a cooling due to pressure lowering and expansion of CO$_2$ (Pruess, 2008). However, the large heat capacity of the rock matrix reduces the extent of these non-isothermal effects and due to the diffusive nature of heat transport, their importance reduces with time.

The cessation of the injection gives rise to a second characteristic time period. Advective flow due to viscous and

buoyant forces slowly decreases. Thus, the relative importance of compositional effects gradually increases, *i.e.*, dissolution of CO$_2$ in the brine phase, increase of the brine density, and downward fingering of the CO$_2$-rich brine. The growing surface of the CO$_2$-phase plume also causes a shift of the governing processes towards compositional effects. This time period is typically expected to be very long, lasting over tens to hundreds of years.

Eventually, multiphase flow processes come to halt. The plume of the CO$_2$-rich phase is immobile and gradually CO$_2$ dissolves into the brine. When considering larger time scales of hundreds to thousands of years, geochemical processes – even with slow kinetics – can become important and affect the properties of the aquifer including porosity and permeability. Since this could potentially trigger new or seal existing flow paths, geochemistry should be considered as interacting with hydraulics, at least in certain sub-domains of the reservoir.

In the modelling of large domains over long periods of time, it can be of substantial benefit to adapt the model complexity both in time and space as required. Sequential model coupling in time and spatial domain decomposition (Toselli and Widlund, 2005) need to be investigated with respect to their application for the simulation of CO$_2$ storage. While domain decomposition is not the subject of the present study, an approach and an application example for a sequential coupling is presented.

2 SEQUENTIAL MODEL COUPLING

Sequential coupling of models has previously been used for the simulation of contaminant spreading in the vadose zone by Class *et al.* (2008). The infiltration of a *light nonaqueous-phase liquid* (LNAPL) into the unsaturated zone, its spreading and transport in the soil air and in the groundwater, as well as a thermally enhanced remediation have been described with a series of three sequentially coupled models.

As discussed in the previous section, the processes which take place during CO$_2$ storage in saline aquifers can also be separated into different time periods. In the following, a sequential coupling concept for the simulation of the non-isothermal flow and transport processes which occur during CO$_2$ storage will be derived. The coupling of geomechanical and geochemical processes will be part of future work.

Two time periods are distinguished here:
– the injection period, and
– the post-injection period.

During the injection period, the CO$_2$-rich phase mainly spreads due to advective and buoyant forces. However, the flow behaviour is also influenced by temperature effects due to an injection temperature that may differ from the reservoir temperature or due to the Joule-Thompson effect. The dissolution and diffusion of CO$_2$ in the brine phase only plays a minor role for the short-term CO$_2$ distribution. Therefore,

the injection period will be described with a nonisothermal two-phase flow model (2*pni* model) that neglects compositional effects.

In the post-injection period, dissolution, diffusion, and density-driven convection become more important while advection- and buoyancy-driven processes slowly decrease. The initial temperature profile slowly reestablishes due to heat conduction and ambient groundwater flow. Thus, the nonisothermal, two-phase flow model needs to be extended to account for compositional effects. This is realised by sequentially coupling a two-phase, two-component model (2*p2cni* model) to the 2*pni* model.

Even though it is not part of this work, it is possible to distinguish an additional time period in which the long-term thermal effects are neglected, further reducing the complexity of the model.

2.1 Mathematical and Numerical Model

In the model of the first time period, *i.e.*, the 2*pni* model, the following mass balance equation is solved for both the wetting brine phase (w) and the nonwetting CO_2-rich phase (*n*):

$$\phi \frac{\partial(\varrho_\alpha S_\alpha)}{\partial t} - \text{div}\left\{\varrho_\alpha \frac{k_{r\alpha}}{\mu_\alpha} \mathbf{K}(\text{grad } p_\alpha - \varrho_\alpha \mathbf{g})\right\}$$
$$- q_\alpha = 0, \qquad \alpha \in \{w, n\}. \qquad (1)$$

Above and in the sequel we use standard notation, Helmig *et al.* (1997), which is also explained in the nomenclature at the beginning of this paper. Additionally, the energy balance equation of the fluid-solid mixture is solved to describe the nonisothermal processes. Assuming local thermal equilibrium, the energy balance equation can be written as follows:

$$\phi \frac{\partial\left(\sum_\alpha \varrho_\alpha u_\alpha S_\alpha\right)}{\partial t} + (1 - \phi) \frac{\partial(\varrho_s c_s T)}{\partial t}$$
$$- \sum_\alpha \text{div}\left\{\varrho_\alpha h_\alpha \frac{k_{r\alpha}}{\mu_\alpha} \mathbf{K}(\text{grad } p_\alpha - \varrho_\alpha \mathbf{g})\right\}$$
$$- \text{div}\left(\lambda_{pm} \text{grad } T\right)$$
$$- q_h = 0 \qquad (2)$$

Where the summation is taken over the phases $\alpha \in \{w, n\}$. To close this system of equations, the following auxiliary conditions are applied:

$$\sum_\alpha S_\alpha = 1 \quad \text{and} \quad p_w = p_n - p_c(S_w) \qquad (3)$$

The model of the second time period (2*p2cni* model) solves compositional mass balances for the components CO_2 and H_2O. It is assumed that the CO_2-rich phase consists of a maximum of two components namely CO_2 and H_2O, whereas the brine phase consists of the three components CO_2, H_2O and halite (NaCl). However, there is no mass balance for NaCl, since the mass fraction of NaCl is assumed

to be constant and determined by the average salinity of the reservoir. The energy equation of the 2*p2cni* model is similar to Equation (2), but the phase enthalpies and internal energies are functions of the dissolved components in addition to pressure and temperature. The component mass balances are described by:

$$\phi \frac{\partial(\sum_\alpha \varrho_\alpha X_\alpha^\kappa S_\alpha)}{\partial t}$$
$$- \sum_\alpha \text{div}\left\{\varrho_\alpha X_\alpha^\kappa \frac{k_{r\alpha}}{\mu_\alpha} \mathbf{K}(\text{grad } p_\alpha - \varrho_\alpha \mathbf{g})\right\}$$
$$- \sum_\alpha \text{div}\left\{\mathbf{D}_{\alpha,\mathbf{pm}}^\kappa \varrho_\alpha \text{grad} X_\alpha^\kappa\right\}$$
$$- \sum_\alpha q_\alpha^\kappa = 0 \qquad \kappa \in \{H_2O, CO_2\}. \qquad (4)$$

Besides the equations given in (3), a further auxiliary condition needs to be fullfilled for each phase in the 2*p2cni* model:

$$\sum_\kappa X_\alpha^\kappa = 1 \qquad (5)$$

The fluid properties of the CO_2-rich phase are calculated as functions of pressure and temperature. The properties of the brine phase additionally depend on the salinity, and in the compositional model, on the CO_2 mass fraction. In the compositional model, the mutual solubilities of brine and CO_2 are calculated as a function of the brine salinity, the pressure and the temperature according to Spycher and Pruess (2005). For further information on the fluid property functions, the reader is referred to Bielinski (2006).

Equations (1, 2), and (4) are discretised with a fully implicit Euler scheme in time and with a vertex-centered finite volume method (BOX method) in space (Helmig *et al.*, 1997). This is implemented in the new multi-scale, multi-physics toolbox DuMu^x (Flemisch *et al.*, 2007, http://www.dumux.de).

2.2 Transfer of Primary Variables and Mass Conservation

The 2*pni* model solves for a constant set of primary variables *i.e.*, the brine-phase pressure p_w, the CO_2 saturation S_n and the temperature T.

The set of primary variables in the 2*p2cni* model, however, changes with the phase state. The phase state is a control volume specific information and can either be *brine phase only*, *CO_2-rich phase only* or *both phases*. If only one phase is present, either brine or CO_2, the value of S_n is constant and a mass fraction is used as primary variable. For a single-phase brine system, the mass fraction of CO_2 in the brine phase is the primary variable. For a single-phase CO_2 system, the mass fraction of H_2O in the CO_2-rich phase is the primary variable. If the mass fraction reaches the

value of maximum solubility X_{eq}^{κ}, a second phase appears, and the primary variable is switched to the CO_2 saturation S_n (*Tab. 1*). For saturation values of 0.0 and 1.0, the model switches back to *brine phase only* or *CO₂-rich phase only*, respectively.

TABLE 1

In the 2*p2cni* model, the set of primary variables depends on the phase state

Primary variables		
Brine phase only	CO₂-rich phase only	Both phases
$p_w, X_w^{CO_2}, T$	$p_w, X_n^{H_2O}, T$	p_w, S_n, T
Mass fraction		
Brine phase only	CO₂-rich phase only	Both phases
$X_w^{CO_2} < X_{eq}^{CO_2}$	$X_n^{H_2O} < X_{eq}^{H_2O}$	$X_w^{CO_2} = X_{eq}^{CO_2}$ $X_n^{H_2O} = X_{eq}^{H_2O}$

During the switch from the 2*pni* model to the 2*p2cni* model, the primary variables need to be transferred on each node of the grid in a way that guarantees the conservation of the CO_2 mass. In regions where only one phase is present in the 2*pni* model, either brine or CO_2, the mass fraction of CO_2 in the brine phase ($X_w^{CO_2}$) or the mass fraction of H_2O in the CO_2-rich phase ($X_n^{H_2O}$) are initialised with zero accordingly in the 2*p2cni* model.

If both phases are present in the 2*pni* model, the CO_2 saturation in the 2*p2cni* model needs to be corrected locally after the model coupling. The reason for the correction is the additional CO_2 mass in the brine phase due to the assumed maximum solubility $X_{eq}^{CO_2}$ (*Tab. 1*). The equality of the CO_2 mass in a given control volume before and after the model coupling leads to the following equation:

$$\{S_n \rho_n\}_{2pni} = \{S_n X_n^{CO_2} \rho_n + S_w X_w^{CO_2} \rho_w\}_{2p2cni} \quad (6)$$

Replacing $\{S_w\}_{2p2cni}$ by inserting the first auxiliary condition (*Eq. 3*) and solving for $\{S_n\}_{2p2cni}$ leads to:

$$\{S_n\}_{2p2cni} = \frac{\{S_n \rho_n\}_{2pni} - \{X_w^{CO_2} \rho_w\}_{2p2cni}}{\{\rho_n X_n^{CO_2} - \rho_w X_w^{CO_2}\}_{2p2cni}} \quad (7)$$

Since the value of S_n is reduced by this transformation, the capillary pressure is lowered, and as a consequence, the value of p_n decreases. A decrease in the CO_2 pressure causes a change in the maximum solubility of CO_2 in the brine phase which also has an influence on the brine density. Thus, a few iterations with updated 2*p2cni* terms on the right hand side are performed for Equation (7).

On the edge of the CO_2 plume, small values of $\{S_n\}_{2pni}$ can occur. These values lead to a negative result for $\{S_n\}_{2p2cni}$ in Equation (7) which means that there is not enough CO_2 present to reach the maximum solubility in

the brine phase. In this case, the phase state in the 2*p2cni* model is set to *brine phase only*, and the CO_2 mass fraction is calculated with the following equation:

$$\{X_w^{CO_2} \rho_w\}_{2p2cni} = \{S_n \rho_n\}_{2pni}$$
$$\{X_w^{CO_2}\}_{2p2cni} = \frac{\{S_n \rho_n\}_{2pni}}{\{\rho_w\}_{2p2cni}} \quad (8)$$

Like in Equation (7), a few iterations are necessary to take the influence of the resulting CO_2 mass fraction on the value of $\{\rho_w\}_{2p2cni}$ into account. This method guarantees the conservation of the CO_2 mass in the system, however, due to the modifications in saturation and composition it does not conserve the mass of H_2O.

3 APPLICATION EXAMPLE

In this section, the implemented sequential coupling concept is tested using an idealised, radially symmetric application example.

The model domain is shown in Figure 2. Taking advantage of the radial symmetry, a 30° slice of the reservoir is modelled. It has a thickness of 20 m and a radius of 800 m. The inner radius of the slice is 0.05 m representing the injection well. The vertical discretisation is 1 m, in radial direction the domain is discretised with 40 cells, whereas the cell size increases exponentially, and in angular direction the discretisation is 7.5°, which leads to a grid of 3 200 hexahedral elements.

The reservoir has a porosity of 0.25 and a permeability of 200 mD in *x-y*-direction and 20 mD in *z*-direction. For the description of the capillary pressure p_c and the relative permeabilities $k_{r\alpha}$ the relations given by Brooks and Corey, 1966, are applied. The Brooks-Corey parameters are set to $\lambda_{BC} = 2$ and $p_d = 5\,000$ Pa. The residual saturations of the brine and the CO_2-rich phase are set to 0.25 and 0.025 respectively. The rock has a density of 2 650 kg/m³ and a heat capacity of 800 J/kg. The heat conductivity of the porous medium is calculated as a function of brine saturation according to Somerton *et al.* (1974):

$$\lambda_{pm}(S_w) = \lambda_{dry} + \sqrt{S_w} \cdot (\lambda_{sat} - \lambda_{dry})$$

where $\lambda_{sat} = 2.7$ W/(m K) and $\lambda_{dry} = 0.32$ W/(m K). The salinity of the brine is 0.1728 kg/kg in the whole domain and is assumed to stay constant.

Initially the pressure and the temperature are determined by the hydrostatic pressure distribution and a geothermal gradient of 0.032 K/m starting at the reservoir bottom with a pressure of 259.74 bar and a temperature of 353.47 K. On the outer boundary, the values of p_w and T are set according to the initial conditions. On the top, bottom, and lateral boundaries, Neumann no-flow boundary conditions are
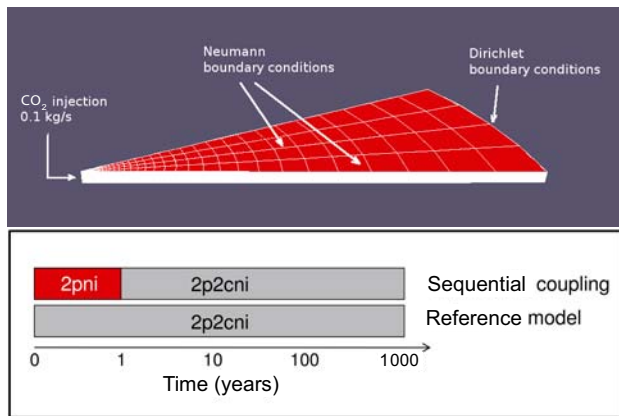
Figure 2

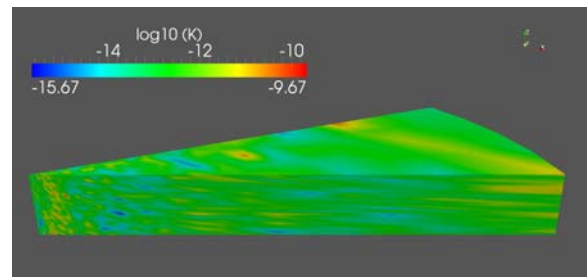Model domain of the application example and sequential coupling scheme.

Figure 3

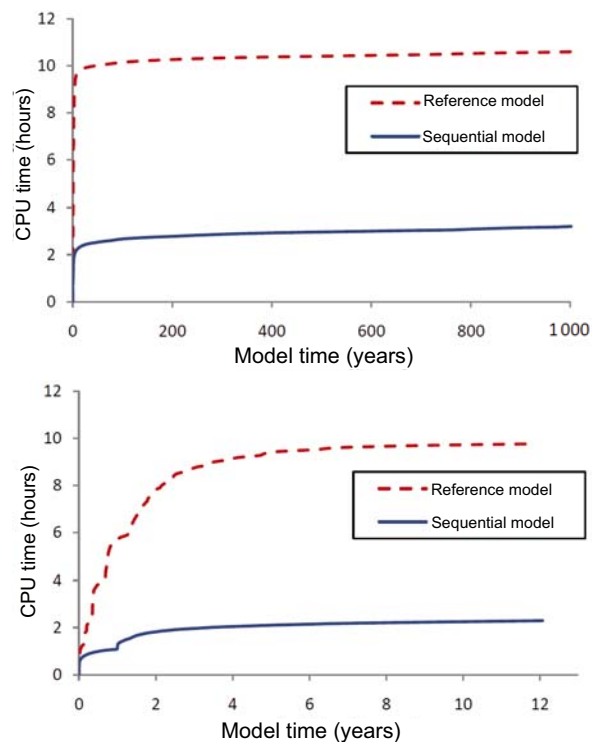Permeability field applied for the heterogeneous application example (z-ratio increased by a factor of 5).

Figure 4

CPU time in hours *versus* simulation time in years for the sequential and the reference model.

applied. The CO_2 is injected at a rate of 0.1 kg/s with a temperature of 308 K for a period of 1 year. After the injection stops, the system is modelled for another 1 000 years.

In the sequentially coupled model, the switch from the $2pni$ to the $2p2cni$ formulation is performed as the injection stops. For comparison, a reference model that applies the $2p2cni$ formulation over the whole timescale is run (*Fig. 2*).

In addition, two variations of the base case example are simulated. The first one applies a grid, which is refined once in radial, angular and vertical direction, leading to 25 600 hexahedral cells. The second one applies a heterogeneous permeability field (*Fig. 3*) created with the geostatistical package gstat (Pebesma, 2004). Even though the examples shown here are far below a realistic scale, they are well-suited to show the general advantages and disadvantages of sequential model coupling. A more detailed study on the effects of heterogeneities, larger geometries, and injection rates will be the subject of future work.

4 DISCUSSION OF THE RESULTS

4.1 Simulation Time

4.1.1 Base Case

In Figure 4, the CPU time is plotted *versus* the simulation time. The simulation of the one-year injection period and the subsequent 1 000 years of relaxation takes 10.59 h with the reference model and 3.19 h with the sequential model on one core of an Intel Core 2 Duo E6300 processor with 1.86 GHz. Thus, the sequential coupling leads to a speed-up of approximately factor 3. As expected, a large speed-up takes place during the injection period, when the less complex $2pni$ formulation is applied in the sequential model. In

addition to its stronger nonlinearities, the reference model is slowed down by the large number of phase switches that occur during this period. The phase switches along with the change of primary variables generally reduce the convergence rate of the Newton algorithm applied in each timestep.

However, the sequentially coupled model also remains faster in the first few years after injection stop (Fig. 4, bottom) even though both models apply the $2p2cni$ formulation at this point. This can be explained by the presence of the single-phase CO_2 region that only develops in the reference model during the injection, the residual brine in the vicinity
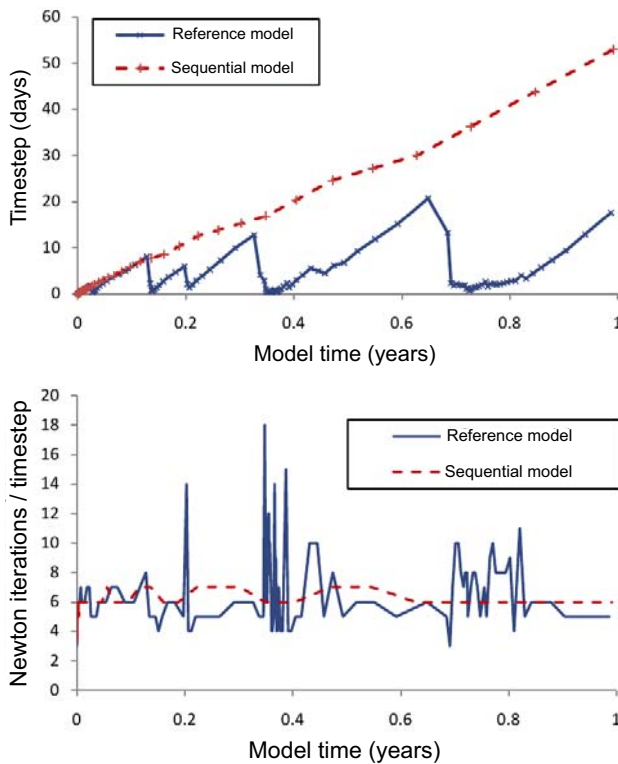
Figure 5

Number of newton iterations per timestep and timestep size for the sequential and the reference models during the injection period.

whereas the refined-grid case required a parallel simulation on eight Intel Xeon E 5440 CPUs with 2.83 GHz. In Table 2 the CPU times for all three cases are shown as well as the speed-up factor. For both, the heterogeneous and the refined-grid case, the speed-up of the sequential model with respect to the reference model is increased compared to the base case. As in the base case, the main speed-up takes place during and shortly after the injection period.

TABLE 2

CPU times (h) of the sequential and the reference models in the three example applications

Case	Sequential model CPU time (h)	Reference model CPU time (h)	Speed-up factor
Base case	3.19	10.59	3.3
Heterogeneous case	4.74	31.64	6.7
Fine-grid case	8.3	38.75	4.7

It is observed, that for both variations the number of newton iterations per timestep in the reference model increases with respect to the base case, which leads to a further reduction of the timestep size (*Fig. 6*). In both cases the reduced convergence of the reference model is caused by a larger number of nodes which encounter a phase switch either due to the finer grid or due to the increased surface area of the plume in the heterogeneous case.

4.2 CO₂ Phase Distribution

In Figure 7 (top), the total CO_2 mass and the mass of CO_2 in the CO_2-rich phase is plotted over time. The total CO_2 mass is the same in both models since the same amount of CO_2 is injected. For the large timescale of 1 000 years, the mass of CO_2 in the CO_2-rich phase calculated by the reference and by the sequential model shows a good agreement.

of the well does not dissolve in the sequential model. After injection stops, this single-phase region gradually dissapears due to brine imbibition. This transformation from a single-phase system to a two-phase system requires an additional number of phase switches in the reference model. Figure 5 (top) shows the timestep size of both models during the injection period. Even though the sequential model is faster due to the less nonlinear equation system that needs to be solved, the main part of the speed-up is caused by the much better convergence and thus the larger timesteps of the 2*pni* model compared to the compositional model during the injection period. This is also shown in Figure 5 (bottom) where the number of newton iterations per timestep is plotted against the model time. Even though another setting of the timestep management can have an influence on the exact value of the resulting speed-up factor, the convergence of the compositional model will always be reduced due to the phase switches.

4.1.2 Refined Grid and Heterogeneities

The simulation of the heterogeneous case is also performed on an Intel Core 2 Duo E6300 processor with 1.86 GHz
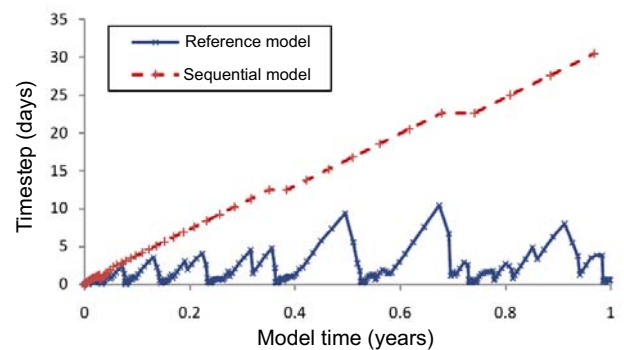

Figure 6

Timestep size for the sequential and the reference models during the injection period modelled on the refined grid.

Figure 7

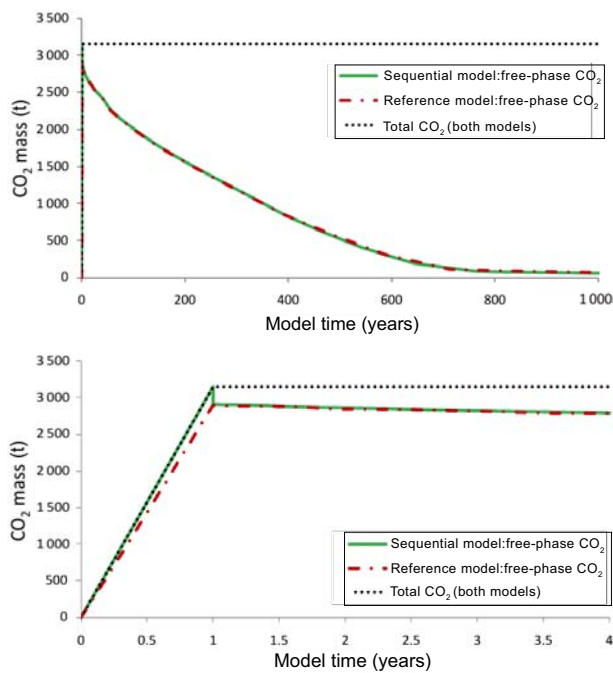Total CO_2 mass and CO_2 mass of the CO_2-rich phase (free-phase CO_2) over time for the sequential and the reference model.
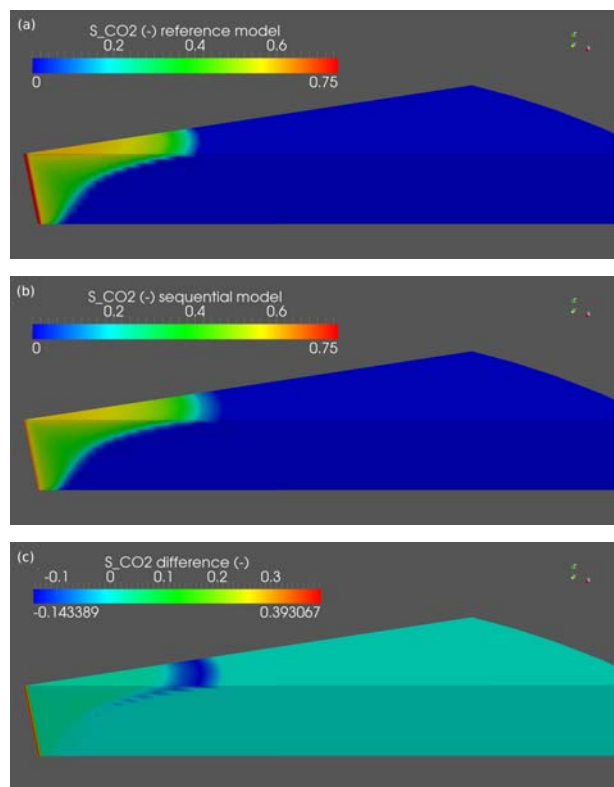

Figure 8

CO_2 saturation distribution after the injection phase for the reference model a) and the sequential model b). In c) the difference in saturation, *i.e.*, the reference model saturation minus the sequential model saturation, is plotted.

If the phase distribution within the first four years is considered (Fig. 7, bottom), small differences between the formulations can be observed. The deviation with respect to the CO_2 mass in the CO_2-rich phase during the first year is caused by the different formulations. In the sequential model, all the CO_2 is in the CO_2-rich phase, while in the reference model, there is already some amount dissolved in the brine phase.

When the injection is shut down, the sequential model switches to the $2p2cni$ formulation. After the switch the phase distributions in both models are in very good agreement.

The refined-grid case and the heterogeneous case show the same behaviour with respect to the CO_2 phase distribution. The phase distribution of CO_2 is an integral measure that is evaluated for the whole reservoir. It does not guarantee that the model results are equal. For a more detailed comparison, the local CO_2 distribution needs to be considered. This is done in the next section.

4.3 Local Differences

4.3.1 CO$_2$ Saturation Distribution

In this and in the next Section the *z*-ratio of the figures is increased by a factor of 5 to also display the vertical CO_2

distribution. Figure 8a, b shows the CO_2 saturation distribution after one year of CO_2 injection for the reference model and the sequential model, respectively. At this point, the switch from the $2pni$ to the $2p2cni$ formulation has already taken place in the sequential model leading to a reduced CO_2 saturation due to the saturation correction (*Sect. 2*). Apart from that, the reference model allows the aforementioned development of a single-phase CO_2 region in the vicinity of the well during the injection period compared to the sequential model which always holds a residual brine phase. The resulting larger CO_2 accumulation of the reference model close to the well leads to a slightly reduced lateral spreading of the plume. In addition to that, the small amount of CO_2 that dissolves in the brine further reduces the plume extent.

These effects can be seen in Figure 8c which shows the resulting saturation difference between the reference and the sequential model. Figure 9 shows the saturation distribution of the reference model and saturation differences compared to the sequential model 100 years after the injection phase. There are still small local saturation differences between the models, however, the maximum difference is 0.015 which
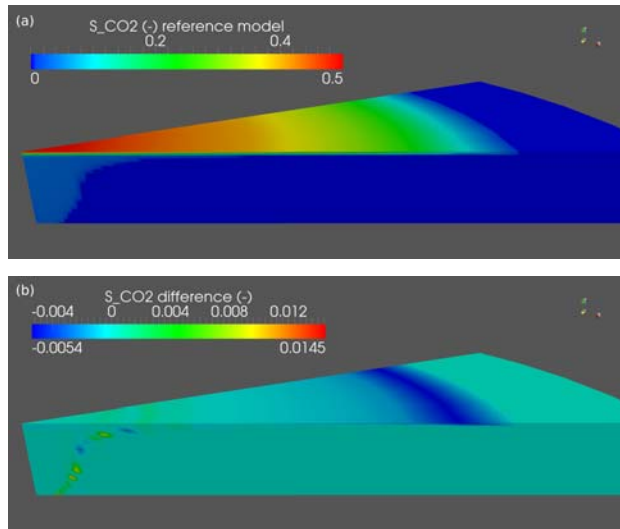
Figure 9

CO$_2$ saturation distribution 100 years after injection stop in the reference model a) and the saturation difference compared to the sequential model b).
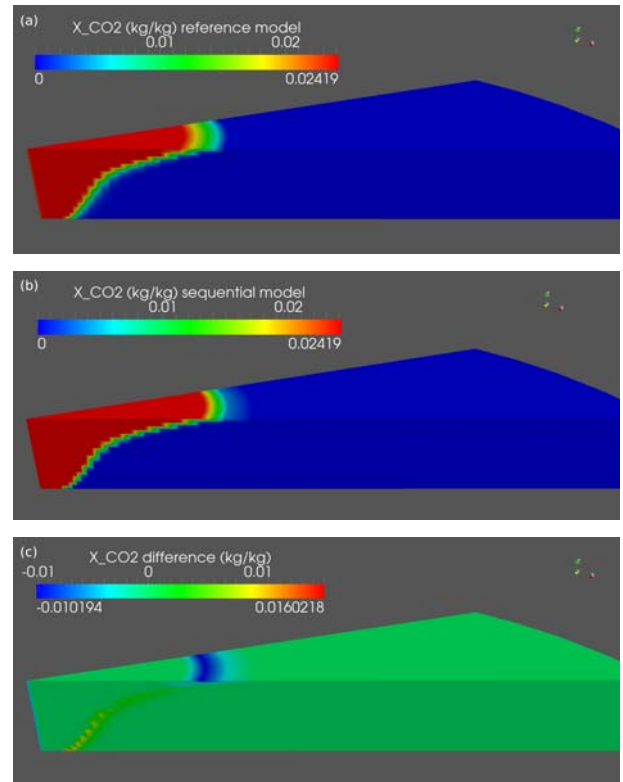

Figure 10

CO$_2$ mass fraction distribution in the reference model a) and in the 2*p2cni* formulation of the sequential model b) after the injection phase. The differences in mass fractions between both models are shown in c).

is more than an order of magnitude less than the saturation differences at the end of the injection phase (*Fig. 8c*).

4.3.2 CO$_2$ Mass Fraction Distribution

Figure 10a, b shows the CO$_2$ mass fraction distribution of the reference model and of the sequential model after the switch from the 2*pni* to the 2*p2cni* formulation. The differences between the models (*Fig. 10c*) result from the differences in the saturation distribution. Thus the plume of dissolved CO$_2$ is slightly larger for the sequential model corresponding to the larger extent of the CO$_2$-phase plume. 1 000 years after the injection phase, almost all the CO$_2$ is dissolved in the brine. Note that only a small amount of CO$_2$ is injected. The heavier, CO$_2$-rich brine leads to the development of density-driven fingering and convective mixing. In Figure 11a, b the mass fraction distribution shows that a large amount of the dissolved CO$_2$ already has sunk to the bottom of the reservoir. The fingering in a homogeneous reservoir like the one regarded here is induced by minimal numerical inaccuracies and is always heavily influenced by the grid. Since the initial mass fraction distribution is not completely the same, the triggering of the convective fingers is not identical either (*Fig. 11c*).

4.3.3 Injection Pressure

With respect to the well-block injection pressure a difference of approximately 0.2 bar can be observed between the reference and the sequential model (*Fig. 12*). In the reference model the injection pressure is smaller since the

injected volume is reduced due to the dissolution of CO$_2$ in the brine phase. As the differences in saturation and mass fraction distribution show, the pressure differences will not have a large effect on the long-term behaviour of the CO$_2$ plume. However, they show that with respect to a pressure study, sequential coupling will lead to an overestimation of the pressure increase. Nevertheless this study is not aiming for an investigation of the injection pressure since this would require to take into account many other factors like the effects of boundary conditions and grid resolution, the compressibility of the rock matrix, and changes in the hydraulic parameters due to mineral precipitation or matrix deformation.

4.3.4 Influence of Grid Refinement and Heterogeneities

For the variations with the refined grid and the heterogeneous intrinsic permeability field the magnitude of local differences between the reference and the sequential model does not increase. In the heterogeneous case the final mass
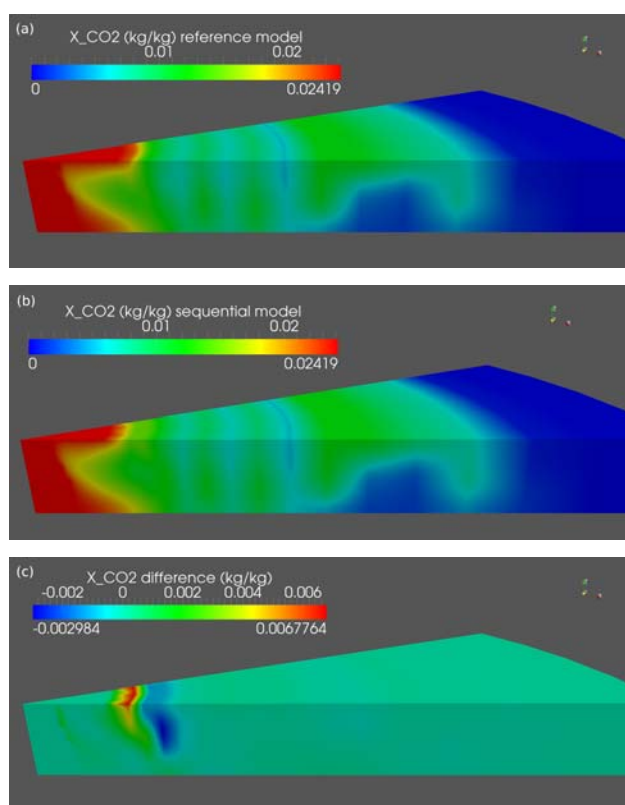
Figure 11

CO_2 mass fraction distribution in the reference model a) and in the sequential model b) 1 000 years after the injection phase. The mass fraction differences between both models are shown in c).

fraction distribution shows less deviations between the reference and the sequential model, since the downward migration is mainly influenced by the heterogeneities and not so much by the shape and the local occurence of the convective fingers.

CONCLUSIONS AND PERSPECTIVES

This study presented a first implementation of a sequential coupling of models of different complexity during and after the injection of CO_2 into a reservoir. It could be shown that:
- the model predictions for the distribution of CO_2, both in phase and dissolved in brine, are in excellent agreement when large time periods are considered;
- the sequentially coupled approach leads to a significant improvement of model efficiency.

It is expected that random processes like the triggering of fingers by instabilities is 'in reality' always dominated by permeability perturbations or local heterogeneities. Thus, the deviations in the mass fraction distributions of dissolved
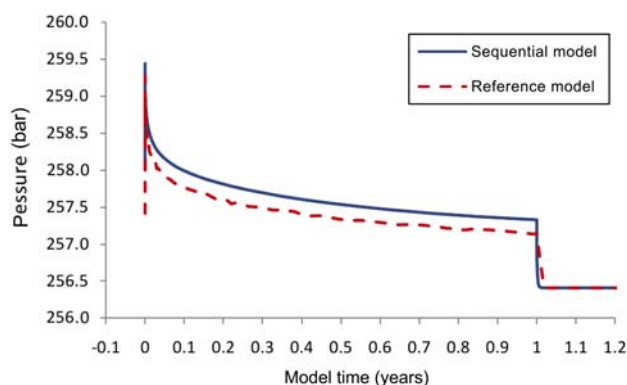

Figure 12

Well-block pressure during the injection period for the reference and the sequential model.

CO_2 are considered as non-limiting for the applicability of the proposed approach.

Both model domain and injection period in this numerical study are far below a realistic scale. Thus, ongoing work is currently concerned with the transfer of these results to relevant spatial and temporal scales. It is of particular importance to develop criteria of 'when' and 'how' such coupling can be done, and what the error introduced by neglecting some of the processes during certain periods is.

ACKNOWLEDGEMENTS

REFERENCES

1 Adrian T., Wendland M., Hasse H., Maurer G. (1998) High-pressure Multiphase Behaviour of Ternary Systems Carbon Dioxide-water-polar Solvent: Review and Modeling with the Pern-Robinson Equation of State, *J. Subercrit. Fluid.* **12**, 185-221.

2 Bielinski A. (2006) Numerical Simulation of CO_2 Sequestration in Geological Formations, *PhD Thesis*, Institut für Wasserbau, Universität Stuttgart.

3 Brooks R.H., Corey A.T. (1966) Properties of Porous Media Affecting Fluid Flow, *J. Irrig. Drain. Division*, 61-88.

4 Class H. *et al.* (2009) A Benchmark-study on Problems Related to CO$_2$ Storage in Geologic Formations - Summary and Discussion of the Results, *Comput. Geosci.* 10.1007/s10596-009-9146-x

5 Class H., Helmig R., Neuweiler I. (2008) Sequential Coupling of Models for Contaminant Spreading in the Vadose Zone. Special Section: Vadose Zone Modeling, *Vadose Zone J.* **7**, 2

6 Darcis M., Class H., Flemisch B. (2009) Coupling Models of Different Complexity for the Simulation of CO$_2$ Storage in Saline Aquifers, *Energy Procedia* **1**, 1767-1774.

7 Flemisch B., Fritz J., Helmig R., Niessner J., Wohlmuth B. (2007) DUMUX: A Multi-scale Multi-physics Toolbox for Flow and Transport Processes in Porous Media, *ECOMAS Thematic Conference on Multi-scale Computational Methods for Solids and Fluids*, Cachan.

8 Helmig R. (1997) *Multiphase Flow and Transport Processes in the Subsurface*, Springer.

9 Metz B., Davidson, O., de Coninck H., Loos M., Meyer L. (2005) IPCC. Special Report on Carbon Dioxide Capture and Storage. *Technical report, Intergovernmental Panel on Climate Change (IPCC)*, Cambridge University Press.

10 Pebesma E.J. (2004) Multivariable geostatistics in S: the gstat package, *Comput. Geosci.* **30**, 683-691.

11 Pruess K. (2008) On CO$_2$ Fluid Flow and Heat Transfer Behavior in the Subsurface, Following Leakage from a Geologic Storage Reservoir, *Environ. Geol.* **54**, 1677-1686.

12 Somerton W.H., El-Shaarani A.H., Mobarak S.M. (1974) High Temperature Behavior of Rocks Associated with Geothermal Type Reservoirs, *Society of Petroleum Engineers*, Paper SPE-4897.

13 Spycher N., Pruess K. (2005) CO$_2$-H$_2$O Mixtures in the Geological Sequestration of CO$_2$. II. Partitioning in Chloride Brines at 12-100°C and up to 600 bar, *Geochim. Cosmochim. Ac.* **69**, 13, 3309-3320.

14 Toselli A., Widlund O.B. (2005) *Domain Decomposition Methods - Algorithms and Theory*, Springer Series in Computational Mathematics **34**.